Revista de la Academia Colombiana de Ciencias Exactas, Físicas y Naturales
48(189):768-783, octubre-diciembre de 2024. doi: https://doi.org/10.18257/raccefyn.2863

Physical Sciences

Original article

Quantum operator for non-paraxial single photon interference

Operador cuántico para la interferencia no-paraxial con fotones individuales

Román Castañeda*, Camilo Hurtado

Physics Department, Universidad Nacional de Colombia, Medellín, Colombia

Abstract

Interference in optics has been described as a result of the superposition of light waves in ordinary space. However, this phenomenological description does not seem to fit non-paraxial single-photon interference in ordinary space due to the corpuscular nature of photons and the fact that only one photon moves in the setup at each time. A quantum interference operator, deduced from the exact (non-paraxial) mathematical model, indicates that the spatial morphology of interference is independent of the presence of photons in the setup and remains unchanged in their absence. This suggests a new interpretation of interference in terms of the photon confinement in geometric states of ordinary space. Here, we discuss the physical and phenomenological implications of this new interpretation.

Keywords: States of space; Geometric potential; Confinement; Spatially structured wells; Vacuum; Interference operator.

Resumen

En óptica la interferencia se ha descrito como resultado de la superposición de ondas de luz en el espacio ordinario. Sin embargo, esta descripción fenomenológica no parece ajustarse a la interferencia no-paraxial con fotones individuales en el espacio ordinario debido a la naturaleza corpuscular de los fotones y a que solo un fotón se mueve en la configuración en cada momento. El operador cuántico de interferencia, deducido del modelo matemático exacto (no-paraxial), indica que la morfología espacial de la interferencia es independiente de la presencia de fotones en la configuración y permanece inalterada en su ausencia. Esto sugiere una nueva interpretación de la interferencia en términos del confinamiento de los fotones en estados geométricos del espacio ordinario. Se discuten aquí las implicaciones físicas y fenomenológicas de esta nueva interpretación de la interferencia.

Palabras clave: Estados del espacio; Potencial geométrico; Confinamiento; Pozos espacialmente estructurados; Vacío; Operador de interferencia.

Introduction

Single photon interference has been of fundamental importance in quantum optics and photonics (**De Martini *et al.***, 1994; **Shih**, 2021) playing a crucial role in the analysis of the quantum properties of light (**Hessmo *et al.***, 2003; **Jones & Wiseman**, 2011), basic quantum phenomena (**Rueckne & Peidle**, 2013; **Tang & Hu**, 2022), and technology development (**Mérolla *et al.***, 1999; **Witkoskie & Cao**, 2008). Due to this wide range of uses and applications, single-photon interference is also considered paradigmatic in education (**Rueckne & Titcomb**, 1996; **Marshman & Singh**, 2017).

The standard quantum formalism predicts experimental outcomes of paraxial single-photon interference. However, it is unsuitable for non-paraxial interference approximation of, and its phenomenological description does not seem to fit the photon corpuscular nature in ordinary space and the fact that only one photon moves in the setup in each experimental realization. This theoretical term denotes the experimental segment that begins with the

Citation: Castañeda R, Hurtado C. Quantum operator for non-paraxial single photon interference. Revista de la Academia Colombiana de Ciencias Exactas, Físicas y Naturales. 48(189):768-783, octubre-diciembre de 2024. doi: https://doi.org/10.18257/raccefyn.2863

Editor: Diógenes Campos Romero

***Corresponding autor:**
Román Castañeda; rcastane@unal.edu.co

Received: July 15, 2024
Accepted: October 28, 2024
Published on line: November 8, 2024

emission of a single photon at the source and ends with its annihilation by the detector so that only this photon propagates in the interferometer without explicit connections with preceding and posterior photons. Consequently, single-photon interference experiments can be theoretically characterized as a binary sequence of only one-particle systems separated by zero-particle systems.

Here, we propose an alternative description developed in the framework of a recently reported non-paraxial quantum formalism of interference with light and single-matter particles (**Castañeda *et al.***, 2023). This new formalism is compatible with the photon corpuscular nature and considers ordinary space as a system with geometric states that confine single photons in spatially distributed zones. In section 2, we deduce a quantum interference operator which includes density operators of the geometric states of space as shown in section 3. In section 4, we discuss the characterization of preparation and measurement (P&M) configured interferometers in terms of geometric states of space, and in section 5, we describe the phenomenology of individual experimental realizations in single-photon interference. Conclusions are summarized in section 6. Details of the mathematical model can be found in the supplementary information.

Quantum interference operator

We show (see Supplementary Information for details) how the non-paraxial Hamiltonian for the electromagnetic field of single photons takes the form

$$H\left(\mathbf{r}_A\right)=\hbar\omega\left(\hat{n}+\frac{1}{2}\right)\int_M\int_M d^2\xi_A\, d^2\xi_D\, \kappa\left(\boldsymbol{\xi}_+,\boldsymbol{\xi}_-\right)\Theta\left(\boldsymbol{\xi}_+,\mathbf{r}_A,\mathbf{z},k\right)\Theta^*\left(\boldsymbol{\xi}_-,\mathbf{r}_A,\mathbf{z},k\right), \quad (1)$$

with $\hbar=\frac{h}{2\pi}$ (h is the Planck constant), ω the photon frequency, and $\hat{n}$ the number operator. It is assumed that single photons propagate between two consecutive planes, M and D, at a distance $|\mathbf{z}|$ (**Figure 1S,** https://www.raccefyn.co/index.php/raccefyn/article/view/2863/4467). Reduced coordinates $\boldsymbol{\xi}_\pm=\boldsymbol{\xi}_A\pm\boldsymbol{\xi}_D/2$ and $\mathbf{r}_\pm=\mathbf{r}_A\pm\mathbf{r}_D/2$ denote pairs of points at M and D, respectively, with the coordinate suffixed A specifying the midpoint between the pair and the coordinate suffixed D denoting their separation vector. For null separation vectors, the reduced coordinates denote single points. Furthermore,

$$\kappa(\boldsymbol{\xi}_+,\boldsymbol{\xi}_-)=\kappa^*(\boldsymbol{\xi}_-,\boldsymbol{\xi}_+)=w(\boldsymbol{\xi}_+,\boldsymbol{\xi}_-)\,\tau(\boldsymbol{\xi}_+,\boldsymbol{\xi}_-)\,cos\left(\beta(\boldsymbol{\xi}_+)\right)cos\left(\beta(\boldsymbol{\xi}_-)\right)cos\left(\theta(\boldsymbol{\xi}_+)-\theta(\boldsymbol{\xi}_-)\right), \quad (2)$$

with $w\left(\boldsymbol{\xi}_+,\boldsymbol{\xi}_-\right)=w^*\left(\boldsymbol{\xi}_-,\boldsymbol{\xi}_+\right)=\psi\left(\boldsymbol{\xi}_+\right)\psi^*\left(\boldsymbol{\xi}_-\right)$ and $\psi\left(\boldsymbol{\xi}\right)$ representing the complex amplitude of probability for single photons at M, $\tau\left(\boldsymbol{\xi}_+,\boldsymbol{\xi}_-\right)=\tau^*\left(\boldsymbol{\xi}_-,\boldsymbol{\xi}_+\right)=t\left(\boldsymbol{\xi}_+\right)t^*\left(\boldsymbol{\xi}_-\right)$ and $t\left(\boldsymbol{\xi}\right)=\left|t\left(\boldsymbol{\xi}\right)\right|\exp\left(i\phi\left(\boldsymbol{\xi}\right)\right)$ the complex transmission function at M, and $\mathbf{e}(\boldsymbol{\xi}_+)\cdot\mathbf{e}(\boldsymbol{\xi}_-)=cos\left(\beta(\boldsymbol{\xi}_+)\right)\,cos\left(\beta(\boldsymbol{\xi}_-)\right)cos\left(\theta(\boldsymbol{\xi}_+)-\theta(\boldsymbol{\xi}_-)\right)$ and $\mathbf{e}\left(\boldsymbol{\xi}_\pm\right)$ the unit photon polarization vector at M. The angles $\beta\left(\boldsymbol{\xi}_\pm\right)$ and $\theta\left(\boldsymbol{\xi}_\pm\right)$ are shown in **figure 2S,** https://www.raccefyn.co/index.php/raccefyn/article/view/2863/4467. Finally (**Castañeda *et al.***, 2020),

$$\Theta\left(\boldsymbol{\xi}_+,\mathbf{r}_+,\mathbf{z},k\right)\Theta^*\left(\boldsymbol{\xi}_-,\mathbf{r}_-,\mathbf{z},k\right)=\left(\frac{k}{4\pi}\right)^2\left(\frac{z+\left|\mathbf{z}+\mathbf{r}_+-\boldsymbol{\xi}_+\right|}{\left|\mathbf{z}+\mathbf{r}_+-\boldsymbol{\xi}_+\right|^2}\right)\left(\frac{z+\left|\mathbf{z}+\mathbf{r}_--\boldsymbol{\xi}_-\right|}{\left|\mathbf{z}+\mathbf{r}_--\boldsymbol{\xi}_-\right|^2}\right)\exp\left(ik\left|\mathbf{z}+\mathbf{r}_+-\boldsymbol{\xi}_+\right|-ik\left|\mathbf{z}+\mathbf{r}_--\boldsymbol{\xi}_-\right|\right), \quad (3)$$

with $k = \omega/c$ and c representing the light speed in the vacuum. Equation (3) defines a non-local, non-paraxial basis where $\Theta\left(\boldsymbol{\xi},\mathbf{r},\mathbf{z},k\right)=-i\frac{k}{4\pi}\left(\frac{z+|\mathbf{z}+\mathbf{r}-\boldsymbol{\xi}|}{|\mathbf{z}+\mathbf{r}-\boldsymbol{\xi}|^2}\right)\exp\left(ik\,|\mathbf{z}+\mathbf{r}-\boldsymbol{\xi}|\right)$ are functions of the Hilbert space corresponding to the coordinate representation of kets $\left|\Theta\left(\boldsymbol{\xi}\right)\right\rangle$, which are labeled for each point at M. Therefore, $\Theta\left(\boldsymbol{\xi}_+,\mathbf{r}_A,\mathbf{z},k\right)\Theta^*\left(\boldsymbol{\xi}_-,\mathbf{r}_A,\mathbf{z},k\right)$ is the coordinate representation of the operator $\left|\Theta(\boldsymbol{\xi}_+)\right\rangle\left\langle\Theta(\boldsymbol{\xi}_-)\right|$, labeled for specific pairs of points at M, i.e., $\left\langle\mathbf{r}_A\left|\Theta(\boldsymbol{\xi}_+)\right\rangle\left\langle\Theta(\boldsymbol{\xi}_-)\right|\mathbf{r}_A\right\rangle=\Theta(\boldsymbol{\xi}_+,\mathbf{r}_A)\Theta^*(\boldsymbol{\xi}_-,\mathbf{r}_A)$. It is apparent that $\left|\Theta\left(\boldsymbol{\xi}_+\right)\right\rangle\left\langle\Theta\left(\boldsymbol{\xi}_-\right)\right|=\left(\left|\Theta\left(\boldsymbol{\xi}_-\right)\right\rangle\left\langle\Theta\left(\boldsymbol{\xi}_+\right)\right|\right)$, i.e., $\left|\Theta\right\rangle\left\langle\Theta\right|$, is a self-adjoint operator.

From the above, the operator

$$\hat{\mathrm{H}}=\hat{\mathrm{H}}^\dagger=\hbar\omega\left(\hat{n}+\frac{1}{2}\right)\int_M\int_M d^2\xi_A\, d^2\xi_D\, \kappa\left(\boldsymbol{\xi}_+,\boldsymbol{\xi}_-\right)\left|\Theta\left(\boldsymbol{\xi}_+\right)\right\rangle\left\langle\Theta\left(\boldsymbol{\xi}_-\right)\right|, \quad (4)$$

Revista de la Academia Colombiana de Ciencias Exactas, Físicas y Naturales
48(189):768-783, octubre-diciembre de 2024. doi: https://doi.org/10.18257/raccefyn.2863

with energy units and † denoting adjointness, is deduced straightforwardly. It should be noted that $\left[\hat{n},\left|\Theta\right\rangle\left\langle\Theta\right|\right]=0$ so that the geometric features of interference described by $\left|\Theta\right\rangle\left\langle\Theta\right|$ are independent of the number of single photons moving in the MD volume. For n individual experimental realizations of single photon interference, this operator determines the non-locality at D

$$\left\langle n,\mathbf{r}_{+}\left|\hat{\mathrm{H}}\right|n,\mathbf{r}_{-}\right\rangle=\hbar\omega\left(n+\frac{1}{2}\right)\int_{M}\int_{M}d^{2}\xi_{A}\;d^{2}\xi_{D}\;\kappa\left(\xi_{+},\xi_{-}\right)\left\langle\mathbf{r}_{+}\left|\Theta\left(\xi_{+}\right)\right\rangle\right\rangle\left\langle\Theta\left(\xi_{-}\right)\left|\mathbf{r}_{-}\right\rangle,\quad(5)$$

and the energy of the recorded photons at each detector pixel

$$\left\langle n,\mathbf{r}_{A}\left|\hat{\mathrm{H}}\right|n,\mathbf{r}_{A}\right\rangle=\hbar\omega\left(n+\frac{1}{2}\right)\int_{M}\int_{M}d^{2}\xi_{A}\;d^{2}\xi_{D}\;\kappa\left(\xi_{+},\xi_{-}\right)\left\langle\mathbf{r}_{A}\left|\Theta\left(\xi_{+}\right)\right\rangle\right\rangle\left\langle\Theta\left(\xi_{-}\right)\left|\mathbf{r}_{A}\right\rangle.\quad(6)$$

Equations (5) and (6) provide an exhaustive description of any individual experimental realization in the preparation-and-measurement configured interferometers, as discussed in the next section. It should be emphasized that Eqs. (5) and (6) do not describe a many-particle system, no matter that n grows arbitrarily. Actually, they describe the formation of single-photon interference patterns as the accumulative outcome of n individual experimental realizations without connections between them, i.e., each realization is strictly an independent only-one-particle system.

Therefore, $\hat{\mathrm{H}}$ in Eq. (4) is the fundamental mathematical concept for the complete quantum description of single-photon interference experiments. We call it the quantum interference operator.

States of space

The binary segments of a single-photon interference experiment are characterized by the sequence $\left\langle 1\left|\hat{n}\right|1\right\rangle=1$, $\left\langle 0\left|\hat{n}\right|0\right\rangle=0$. In the absence of photons, Eq. (4) gives

$$\hat{\mathrm{H}}_{0}=\left\langle 0\left|\hat{\mathrm{H}}\right|0\right\rangle=\frac{1}{2}\hbar\omega\int_{M}\int_{M}d^{2}\xi_{A}\;d^{2}\xi_{D}\;\kappa\left(\xi_{+},\xi_{-}\right)\left|\Theta\left(\xi_{+}\right)\right\rangle\left\langle\Theta\left(\xi_{-}\right)\right|,\quad(7)$$

which is quite different from the standard paraxial approximation result (**Walls & Milburn**, 1995). The significant novelty evidenced by Eq. (7) is that the non-paraxial geometric features of interference remain in the vacuum, i.e., in the absence of photons in the setup. More precisely, they seem to be independent of the presence of photons, thus remaining unchanged along the binary sequence of the experiment. Hence, ordinary space seems to be a system with geometric states of the vacuum energy $\hbar\omega/2$, described by the density operator $\left|\Theta\right\rangle\left\langle\Theta\right|$ (**Castañeda *et al.***, 2023). The contrast between this conception of ordinary space and the Newtonian description in the standard interference formalisms opens the way for the community to discuss the role of ordinary space in interference.

Besides, coefficient $\kappa\left(\xi_{+},\xi_{-}\right)$ in Eq. (7) behaves as a filter placed at M that selects and weights the geometric states of space in the vacuum, thus characterizing each specific interferometer. Such a filter (defined in Eq. (2)) is realized by the interference device, usually a mask, with the effective non-local transmission $\tau_{eff}\left(\xi_{+},\xi_{-}\right)=\tau\left(\xi_{+},\xi_{-}\right)\cos\left(\beta\left(\xi_{+}\right)\right)\cos\left(\beta\left(\xi_{-}\right)\right)\cos\left(\theta\left(\xi_{+}\right)-\theta\left(\xi_{-}\right)\right)$ under the prepared non-locality $w\left(\xi_{+},\xi_{-}\right)$. This role of the setup in the absence of photons invites us to revisit the phenomenological fundamentals of quantum mechanics (**Bohr**, 1935) considering that the interpretation above does not result from heuristic assumptions but from the direct phenomenological analysis of the mathematical model.

To determine the geometric states of space in the quantum interference operator in the vacuum, it is useful to introduce the dimensionless function $1\equiv\delta\left(\xi_{D}\right)+\left(1-\delta\left(\xi_{D}\right)\right)$ in the integrand of Eq. (7), with $\delta\left(\xi_{D}\right)$ as the Dirac delta function, resulting in:

$$\hat{\mathrm{H}}_{0}=\frac{1}{2}\hbar\omega\int_{M}d^{2}\xi_{A}\;\hat{W}\left(\xi_{A}\right)=\frac{1}{2}\hbar\omega\int_{M}d^{2}\xi_{A}\left(\hat{R}\left(\xi_{A}\right)+\frac{1}{2}\hat{G}\left(\xi_{A}\right)\right),\quad(8)$$

where $\hat{W}\left(\xi_{A}\right)=\hat{W}^{\dagger}\left(\xi_{A}\right)=\hat{R}\left(\xi_{A}\right)+\frac{1}{2}\hat{G}\left(\xi_{A}\right)$ is the density operator of excited states of space (**Castañeda *et al.***, 2023),

$$\hat{R}(\xi_A) = \hat{R}^{\dagger}(\xi_A) = \kappa(\xi_A,\xi_A)\left|\Theta(\xi_A)\right\rangle\left\langle\Theta(\xi_A)\right| = \left|\psi(\xi_A)\right|^2\left|t(\xi_A)\right|^2\cos^2\left(\beta(\xi_A)\right)\left|\Theta(\xi_A)\right\rangle\left\langle\Theta(\xi_A)\right| \quad (9)$$

provided by the term $\delta(\xi_D)$, is the density operator of ground states of space labeled at the points ξ_A of M, and

$$\hat{G}(\xi_A) = \hat{G}^{\dagger}(\xi_A) = \int_{\substack{M\\ \xi_D\neq 0}} d^2\xi_D\ \kappa(\xi_+,\xi_-)\left|\Theta(\xi_+)\right\rangle\left\langle\Theta(\xi_-)\right|, \quad (10)$$

given by the term $1-\delta(\xi_D)$, is the density operator of non-local geometric excitation modes called the geometric potential operator (**Castañeda *et al.***, 2023). The density operators $\hat{R}$ and $\hat{G}$ are independent from each other.

In Eq. (9), $0\le\left|t(\xi_A)\right|^2\le 1$ denotes the transmittance of M without polarizers (**Born & Wolf**, 1993) while $\left|t(\xi_A)\right|^2\cos^2\left(\beta(\xi_A)\right)$ represents the effective transmittance with polarizers. Therefore, the coefficient $\left|\psi(\xi_A)\right|^2\left|t(\xi_A)\right|^2\cos^2\left(\beta(\xi_A)\right)$ determines the quantum probability of finding a single photon emerging from ξ_A (see Supplementary Information for details). In turn, each non-local mode $\left|\Theta(\xi_+)\right\rangle\left\langle\Theta(\xi_-)\right|$ of $\hat{G}(\xi_A)$ in Eq. (10) provides the same geometrical excitation at the same time to the ground states of space labeled at the pair of M points $\xi_\pm = \xi_A \pm \xi_D/2$. The excitation is activated by the non-locality $\kappa(\xi_+,\xi_-)$ that links these points. Thus, each individual ground state of space should be geometrically excited by $\frac{1}{2}\hat{G}(\xi_A)$. So, $\hat{G}$ involves the spectrum of spatial modulations that excite the ground states of space $\hat{R}$ and produce the excited geometric states $\hat{W}$. Such spectrum is filtered (selected and weighted) by the non-locality at M for any single photon interferometer and it is not activated if $\kappa(\xi_+,\xi_-)=0$ for any $\xi_D\neq 0$. In this case, none of the ground states of space are excited so that the geometric states of space reduce to the ground states, i.e., $\hat{W}(\xi_A)=\hat{R}(\xi_A)$.

Preparation and measurement scheme

Space states for non-locality preparation

Figure 1 depicts the conceptual configuration of single-photon interference setups, in other words, the P&M scheme. Equation (8) gives the interference operator in the vacuum for the MD stage and, after expressing it as reduced coordinates of the SM stage, it also gives the interference operator in the vacuum for this stage. However, the geometric potential is not activated in the SM stage because the individual experimental realizations of single-photon interference experiments are independent of each other. Therefore, only ground states of space are established in the SM stage, so that,

$$\hat{\mathrm{H}}_0 = \frac{\hbar\omega}{2}\int_S d^2r'_A\,\hat{W}(\mathbf{r}'_A) = \frac{\hbar\omega}{2}\int_S d^2r'_A\,\hat{R}(\mathbf{r}'_A) = \frac{\hbar\omega}{2}\int_S d^2r'_A\left|\psi(\mathbf{r}'_A)\right|^2\left|t(\mathbf{r}'_A)\right|^2\cos^2\left(\beta(\mathbf{r}'_A)\right)\left|\Theta(\mathbf{r}'_A)\right\rangle\left\langle\Theta(\mathbf{r}'_A)\right| \quad (11)$$

The projection of the interference operator in Eq. (11) on pairs of points at M gives the prepared non-locality at M $w(\xi_+,\xi_-)=\left\langle\xi_+\right|\hat{\mathrm{H}}_0\left|\xi_-\right\rangle=\frac{\hbar\omega}{2}\int_S d^2r'_A\left\langle\xi_+\right|\hat{R}(\mathbf{r}'_A)\left|\xi_-\right\rangle$, with

$$\left\langle\xi_+\right|\hat{R}(\mathbf{r}'_A)\left|\xi_-\right\rangle = \left(\frac{k}{4\pi}\right)^2\left|\psi(\mathbf{r}'_A)\right|^2\left|t(\mathbf{r}'_A)\right|^2\cos^2\left(\beta(\mathbf{r}'_A)\right)\left(\frac{z'+\left|\mathbf{z}'+\xi_+-\mathbf{r}'_A\right|}{\left|\mathbf{z}'+\xi_+-\mathbf{r}'_A\right|^2}\right) \times\left(\frac{z'+\left|\mathbf{z}'+\xi_--\mathbf{r}'_A\right|}{\left|\mathbf{z}'+\xi_--\mathbf{r}'_A\right|^2}\right)\exp\left(ik\left|\mathbf{z}'+\xi_+-\mathbf{r}'_A\right|-ik\left|\mathbf{z}'+\xi_--\mathbf{r}'_A\right|\right). \quad (12)$$

Remarkably, non-locality at S is not required to prepare non-locality at M. Moreover, only one ground state of space can prepare the non-locality $w(\xi_+,\xi_-)=\left\langle\xi_+\right|\hat{\mathrm{H}}_0\left|\xi_-\right\rangle=\frac{\hbar\omega}{2}\left\langle\xi_+\right|\hat{R}(\mathbf{r}'_A)\left|\xi_-\right\rangle$ at M, as illustrated in **figure 2**. This exact numerical simulation points out

Revista de la Academia Colombiana de Ciencias Exactas, Físicas y Naturales
48(189):768-783, octubre-diciembre de 2024. doi: https://doi.org/10.18257/raccefyn.2863

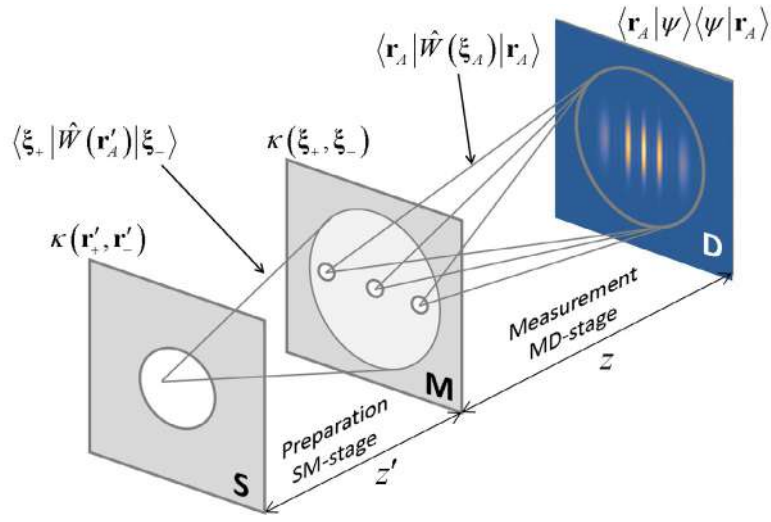

Figure 1. Conceptual sketch of the single-photon interference setup in the preparation-and-measurement (P&M) scheme. The expressions are explained in the text.

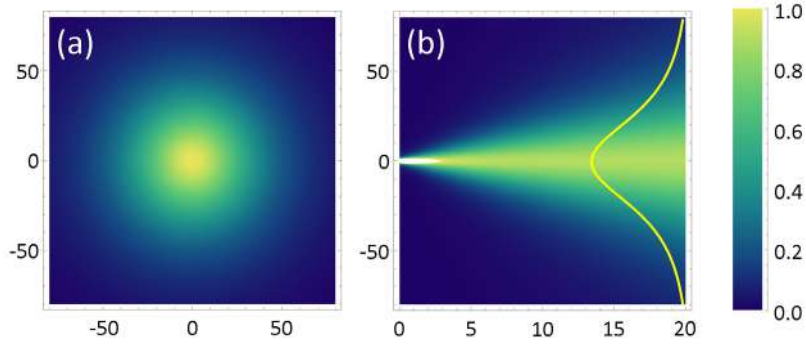

Figure 2. Non-locality Lorentzian cone for a single ground state of space prepared in the SM-stage in **figure 1**. **(a)** Cross-section at z'=50λ (λ = 0.4 μm) and **(b)** axial section for $0 \leq z' \leq 50\lambda$. The Well vertex is at $r'_A = 0$ on S. Non-locality support centered at $\xi_A = 0$ on M is described by **(a)** and the vertical profile in **(b)**. The horizontal and vertical axes are the Cartesian components of ξ_D in **(a)**, and z' and mutually parallel components of r'_A on the left side and ξ_D on the right side in **(b)**. Axes units are μm and the scale is in dimensionless arbitrary units.

that Eq. (12) describes cones in ordinary space with vertices at specific $\mathbf{r}'_A$ points on S, the bases on the pairs of M points $\xi_\pm$ of the region centered at a given ξ_A and Lorentzian cross-sections at any distance from S. The cone effective angular aperture is ~80°.

The prepared non-locality $w(\xi_+,\xi_-) = \langle \xi_+|\hat{\mathrm{H}}_0|\xi_-\rangle$ corresponds to the cross-section at M of the overlapped ground states in Eq. (11). The area of the cross-section centered at ξ_A, where the prepared non-locality takes on non-negligible values, determines its support (**Castañeda *et al.***, 2023) and specifies the non-locality links between pairs of points $\xi_\pm$ symmetrically distributed to ξ_A. Such links are negligible or nullified for pairs of points with separation vectors longer than the non-locality support diameter.

We emphasize that the ground states establish Lorentzian cones in ordinary space for the non-locality preparation and are compatible with the local nature of the photon emissions by the source. Indeed, the factor $|\psi(\mathbf{r}'_A)|^2\,|t(\mathbf{r}'_A)|^2\cos^2(\beta(\mathbf{r}'_A))$ in Eq. (12) determines the quantum probability for a single photon to be emitted at cone vertex $\mathbf{r}'_A$. However, the preparation of such quantum probability does not require the presence of photons in the setup.

The set of ground states of space with vertices at the emitting points of an extended photon source is non-separable. The complex-valued function in Eq. (12) is non-factorable and given its harmonic factor, Eq. (11) implies that each ground state is spatially modulated by the remaining ones. Consequently, non-locality spatially structured Lorentzian cones, as illustrated in **figure 3**, work for spacing the vertex array longer than λ in (a)-(c) and shorter than λ in (d)-(f). Given the non-separability of ground states for the non-locality preparation, the set associated with all the emitting points should be included in the integral of Eq. (11), no matter that the emission of the single photon in any individual experimental realization is a local event occurring at a specific source point.

Now, the $\hat{R}(\mathbf{r}'_A)$ projection on individual M points gives the real-valued, positive, definite, and separable functions

$$\langle \xi_A | \hat{R}(\mathbf{r}'_A) | \xi_A \rangle = \left(\frac{k}{4\pi} \right)^2 |\psi(\mathbf{r}'_A)|^2 \, |t(\mathbf{r}'_A)|^2 \, \cos^2(\beta(\mathbf{r}'_A)) \left(\frac{z' + |\mathbf{z}' + \xi_A - \mathbf{r}'_A|}{|\mathbf{z}' + \xi_A - \mathbf{r}'_A|^2} \right)^2, \quad (13)$$

that determine a Lorentzian cone in the SM stage, with angular aperture of ~70° and vertex at the emission point $\mathbf{r}'_A$, so that $\langle \xi_A | \hat{R}(\mathbf{r}'_A) | \xi_A \rangle$ takes the form $|\psi(\mathbf{r}'_A)|^2 \, |t(\mathbf{r}'_A)|^2 \, \cos^2(\beta(\mathbf{r}'_A))$ as $\mathbf{z}' \to 0$, as illustrated in **figure 4**. It is worth noting that the complex-valued function in Eq. (12) cannot determine an observable so the prepared non-locality at M in Eq. (11)

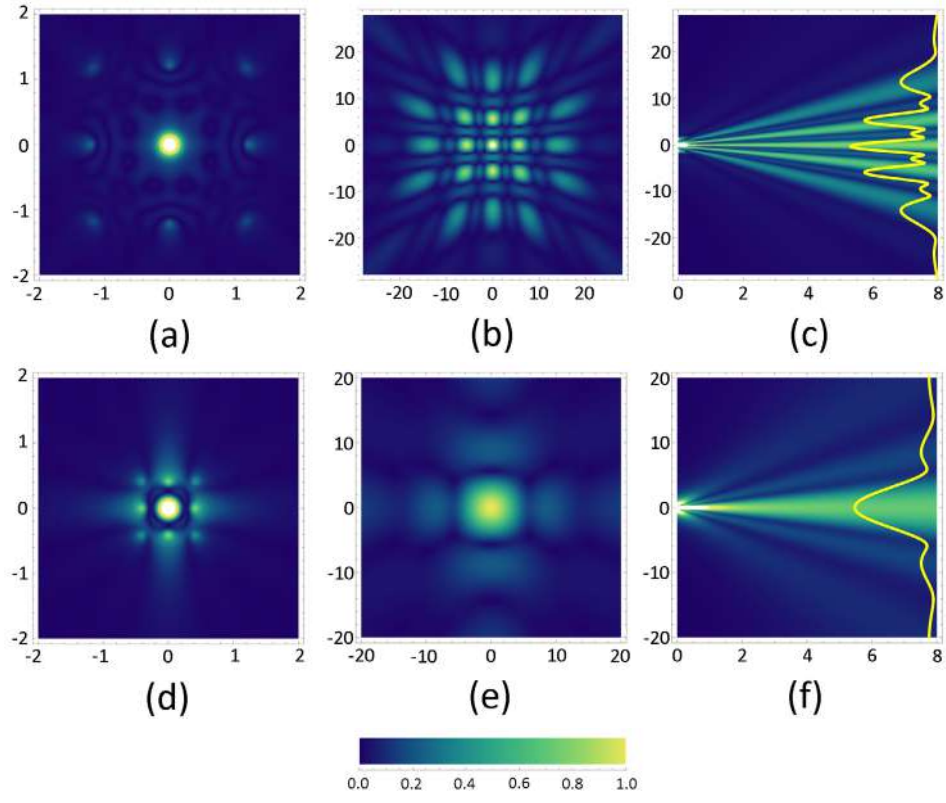

Figure 3. Spatially structured non-locality cones established by an array of 3x3 ground states of space in the SM stage of the setup in **figure 1**. Horizontal and vertical array spacing are 1.5λ in (a)-(c) and 0.5λ in (d)-(f) ($\lambda = 0.4\mu m$). Cross-sections at $z' = 0.1\lambda$ on the left column, $z' = 20\lambda$ on the central column, and axial sections for $0 \leq z' \leq 20\lambda$ on the right column. Cone vertices are at the 3x3 array of emitting points at S and their basis is centered at $\xi_A = 0$ on M. Prepared non-locality supports are described by graphs on the central column and vertical profiles on the right column. Horizontal and vertical axes of cross-sections are the components of the separation vectors ξ_D. Axial-section axes are z' (horizontal) and mutually parallel components of $\mathbf{r}'_A$ on the left vertical edge and ξ_D on the right one. The axes units are μm and the scale is in dimensionless arbitrary units.

Revista de la Academia Colombiana de Ciencias Exactas, Físicas y Naturales
48(189):768-783, octubre-diciembre de 2024. doi: https://doi.org/10.18257/raccefyn.2863

is not measurable by a square modulus detector. In contrast, Eq. (13) characterizes such observable by determining the quantum probability of finding the emitted single photon at any point $\boldsymbol{\xi}_A$ of M in each experimental realization, as

$$\left|\psi\left(\boldsymbol{\xi}_A\right)\right|^2 = \left\langle \boldsymbol{\xi}_A \left| \hat{\mathrm{H}}_0 \right| \boldsymbol{\xi}_A \right\rangle = \frac{\hbar\omega}{2} \left\langle \boldsymbol{\xi}_A \left| \hat{R}\left(\mathbf{r}'_A\right) \right| \boldsymbol{\xi}_A \right\rangle. \tag{14}$$

Nevertheless, the vertex position of this Lorentzian cone is restricted by the geometric uncertainty in the sense that it can be any point within an area of diameter $\lambda/10$ around each S point $\mathbf{r}'_A$ (**Castañeda *et al.***, 2020; 2023).

The numerical simulation of the exact (non-paraxial) Eq. (14) in **figure 4** has some important phenomenological implications: (i) it is compatible with a corpuscular characterization of the single photon; (ii) its Lorentzian profile distributes the quantum probability of emission in a conical volume maintaining the largest probability along the cone axis; therefore, the cross-section in **figure 4 (a)** describes the expectation of single photon measurements at M; (iii) once the SM stage is configured, all the $\left\langle \boldsymbol{\xi}_A \left| \hat{R}\left(\mathbf{r}'_A\right) \right| \boldsymbol{\xi}_A \right\rangle$ functions are established with the same geometry, given by $\left(\frac{k}{4\pi}\right)^2 \left(\frac{z' + \left|\mathbf{z}' + \boldsymbol{\xi}_A - \mathbf{r}'_A\right|}{\left|\mathbf{z}' + \boldsymbol{\xi}_A - \mathbf{r}'_A\right|^2}\right)^2$.

These features suggest that $\left\langle \boldsymbol{\xi}_A \left| \hat{R}\left(\mathbf{r}'_A\right) \right| \boldsymbol{\xi}_A \right\rangle$ determines a Lorentzian well for single photon propagation from each emitting S point to any M point. Such Lorentzian well confines the photon preferably around the axis. This description is supported by a rigorous exact (non-paraxial) deduction and the confinement pins down the unrestricted spatial behavior attributed to the photons by the paraxial approximated formalism, thus increasing the accuracy of the description.

Space states for interference measurement

The quantum interference operator in the vacuum (Eq. (8)) gives the quantum probability for single photon arrivals to the detector pixel at any $\mathbf{r}_A$ point of D as follows:

$$\begin{aligned} \left|\psi\left(\mathbf{r}_A\right)\right|^2 &= \left\langle \mathbf{r}_A \left| \hat{\mathrm{H}}_0 \right| \mathbf{r}_A \right\rangle = \frac{\hbar\omega}{2} \int_M d^2\xi_A \left\langle \mathbf{r}_A \left| \hat{W}\left(\boldsymbol{\xi}_A\right) \right| \mathbf{r}_A \right\rangle \\ &= \frac{\hbar\omega}{2} \int_M d^2\xi_A \left(\left\langle \mathbf{r}_A \left| \hat{R}\left(\boldsymbol{\xi}_A\right) \right| \mathbf{r}_A \right\rangle + \frac{1}{2} \left\langle \mathbf{r}_A \left| \hat{G}\left(\boldsymbol{\xi}_A\right) \right| \mathbf{r}_A \right\rangle \right), \end{aligned} \tag{15}$$

where the ground states of space establish the Lorentzian wells

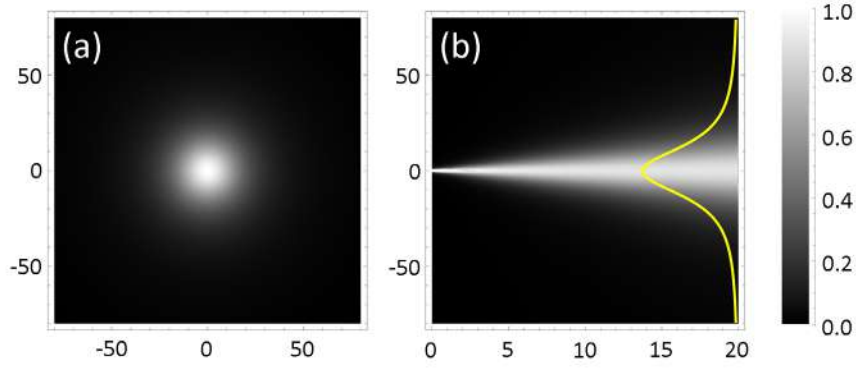

Figure 4. The Lorentzian well for a single ground state of space in the SM stage of **figure 1**. **(a)** Cross-section at $z' = 50\lambda$ ($\lambda = 0.4\mu m$) and **(b)** axial section for $0 \leq z' \leq 50\lambda$. The well vertex is at $\mathbf{r}'_A = 0$ on S. The vertical profile in **(b)** shows the Lorentzian profile of the cross-section. Horizontal and vertical axes are the Cartesian components of $\boldsymbol{\xi}_A$ in **(a)**, z' and the mutually parallel components of $\mathbf{r}'_A$ on the left side, and $\boldsymbol{\xi}_A$ on the right side in **(b)**. Axes units are μm and the scale is in dimensionless arbitrary units.

$$\left\langle \mathbf{r}_A \left| \hat{R}(\xi_A) \right| \mathbf{r}_A \right\rangle = \left(\frac{k}{4\pi} \right)^2 \left| \psi(\xi_A) \right|^2 \left| t(\xi_A) \right|^2 \cos^2\left(\beta(\xi_A) \right) \left(\frac{z + \left| \mathbf{z} + \mathbf{r}_A - \xi_A \right|}{\left| \mathbf{z} + \mathbf{r}_A - \xi_A \right|^2} \right)^2 \quad (16)$$

in the MD stage, as illustrated in **figure 5**, and the geometric potential provides the excitation

$$\begin{aligned} \left\langle \mathbf{r}_A \left| \hat{G}(\xi_A) \right| \mathbf{r}_A \right\rangle &= \int_{\substack{M \\ \xi_D \neq 0}} d^2\xi_D \, \kappa(\xi_+, \xi_-) \left\langle \mathbf{r}_A \left| \Theta(\xi_+) \right\rangle \right\langle \Theta(\xi_-) \left| \mathbf{r}_A \right\rangle \\ &= 2 \int_{\substack{M \\ \xi_D \neq 0}} d^2\xi_D \left| \kappa(\xi_+, \xi_-) \right| \mathrm{Re}\left[\left\langle \mathbf{r}_A \left| \Theta(\xi_+) \right\rangle \right\langle \Theta(\xi_-) \left| \mathbf{r}_A \right\rangle \exp\left(i\alpha(\xi_+, \xi_-) \right) \right]. \end{aligned} \quad (17)$$

In Eq. (17), Re denotes the real part and the following features are considered: (i) $\kappa(\xi_+, \xi_-) = \left| \kappa(\xi_+, \xi_-) \right| \exp\left(i\alpha(\xi_+, \xi_-) \right)$; (ii) the Hermitian symmetry of integrand in Eq. (10) for permutation $\pm\xi_D \to \mp\xi_D$, and (iii) the addition of the integrand terms for the two degrees of freedom in the orientation of the separation vector, i.e., $\pm\xi_D$. Therefore, the geometric potential $\left\langle \mathbf{r}_A \left| \hat{G}(\xi_A) \right| \mathbf{r}_A \right\rangle$ is real valued and takes on positive and negative values, as illustrated in **figure 6 (a)-(c)**.

Equation (15) reduces to $\left| \psi(\mathbf{r}_A) \right|^2 = \left\langle \mathbf{r}_A \left| \hat{\mathrm{H}}_0 \right| \mathbf{r}_A \right\rangle = \frac{\hbar\omega}{2} \int_M d^2\xi_A \left\langle \mathbf{r}_A \left| \hat{R}(\xi_A) \right| \mathbf{r}_A \right\rangle$ if $\kappa(\xi_+, \xi_-) = 0$ for $\xi_D \neq 0$, and Eq. (16) points out that the Lorentzian wells cannot spatially modulate each other by overlapping in $\left\langle \mathbf{r}_A \left| \hat{\mathrm{H}}_0 \right| \mathbf{r}_A \right\rangle$, as illustrated in **figure 5**. Therefore, the geometric potential is necessary and sufficient to excite the ground states, thus producing the spatially structured Lorentzian wells $\left\langle \mathbf{r}_A \left| \hat{W}(\xi_A) \right| \mathbf{r}_A \right\rangle = \left\langle \mathbf{r}_A \left| \hat{R}(\xi_A) \right| \mathbf{r}_A \right\rangle + \frac{1}{2} \left\langle \mathbf{r}_A \left| \hat{G}(\xi_A) \right| \mathbf{r}_A \right\rangle$ required for interference, as those illustrated in **figure 6**, and implying $\kappa(\xi_+, \xi_-) \neq 0$ for $\xi_D \neq 0$.

We emphasize that both the vertex position of the geometric states of space and the excitation provided by the geometric potential are restricted by the geometric uncertainty (**Castañeda *et al.***, 2020; 2023). The vertex position can be any point within an area of diameter $\lambda/10$ around each considered point ξ_A of M, and the geometric potential cannot excite the space states whose vertex separation is no longer than $\lambda/10$. Consequently, such an area is associated with a unique ground state of space with a vertex at any point within the area. It has been shown that this geometric uncertainty cannot be removed or reduced.

Due to the geometric uncertainty, the configuration of the mask placed at M, and the prepared non-locality on this plane, a discrete and finite set of geometric states of space is established in the MD stage of the setup. This set is filtered (selected and weighted) by the non-locality $\kappa(\xi_+, \xi_-)$. More precisely, its local component for $\xi_D = 0$, $\kappa(\xi_A, \xi_A) = \left| \psi(\xi_A) \right|^2 \left| t(\xi_A) \right|^2 \cos^2\left(\beta(\xi_A) \right)$ determines the quantum probability

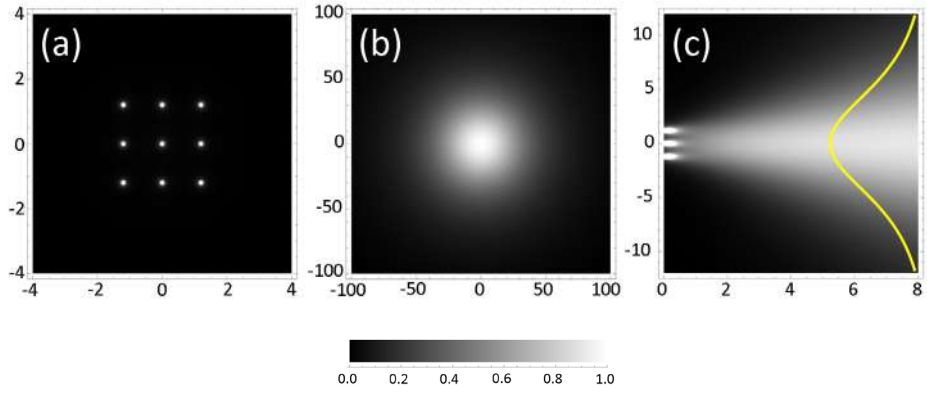

Figure 5. Lorentzian well provided by an array of 3x3 base states of space in the MD stage. **(a)** Array of vertex points at M with horizontal and vertical spacing of $a = 3\lambda$ ($\lambda = 0.4\mu m$). **(b)** Cross-section at $z = 100\lambda$. **(c)** Axial sections for $0 \leq z \leq 20\lambda$. Horizontal and vertical axes: **(a)**, **(b)** Cartesian components of $\mathbf{r}_A$, **(c)** z and mutually parallel Cartesian components of ξ_A at the left edge and $\mathbf{r}_A$ at the right edge. Axes units are expressed in μm and the scale is in dimensionless arbitrary units.

Revista de la Academia Colombiana de Ciencias Exactas, Físicas y Naturales
48(189):768-783, octubre-diciembre de 2024. doi: https://doi.org/10.18257/raccefyn.2863

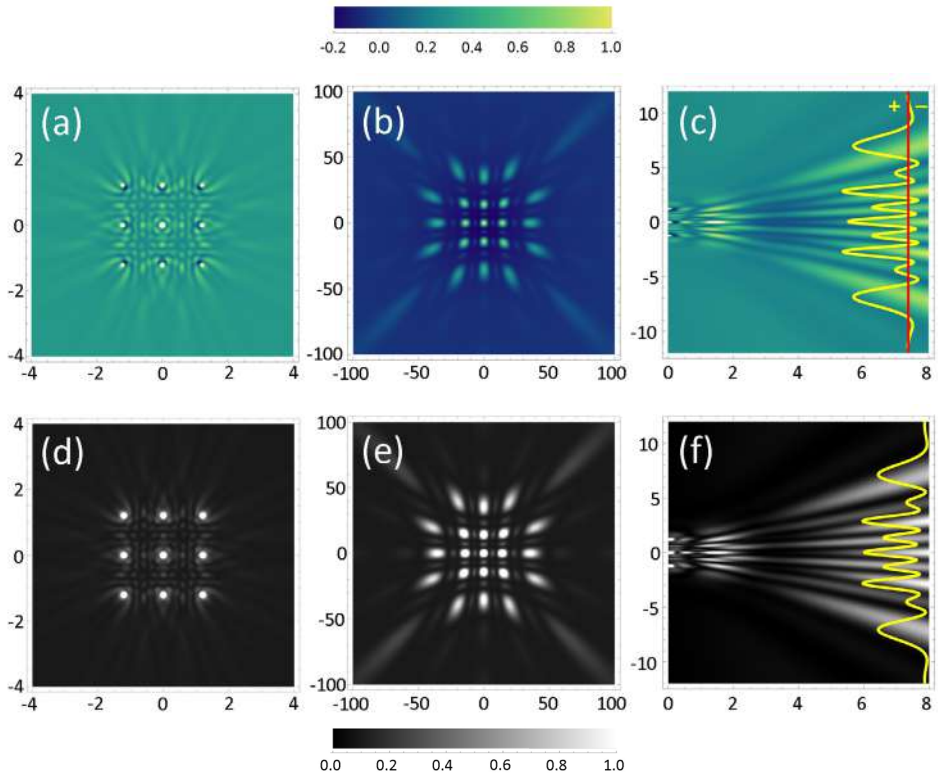

Figure 6. Cross-sections (left and central columns) and axial sections (right column) of the geometric potential on the top row and the spatially structured Lorentzian wells on the bottom row of the example in **figure 5** under a maximum prepared non-locality at M

that filters the set of ground states while its non-local component for $\xi_D \neq 0$, $\kappa(\xi_+,\xi_-)=w(\xi_+,\xi_-)\,\tau(\xi_+,\xi_-)\cos(\beta(\xi_+))\cos(\beta(\xi_-))\cos(\theta(\xi_+)-\theta(\xi_-))$ filters the set of geometric potential modes that excite these ground states. Such excitations only configure specific distributions of zones of non-null quantum probability in the volume of the Lorentzian wells. Thus, spatially structured Lorentzian wells are established in the MD stage where the concentration of quantum probability characterizes the confinement zones. However, the spatially-structured Lorentzian well of each geometric state of space, $\langle \mathbf{r}_A|\hat{W}(\xi_A)|\mathbf{r}_A\rangle=\langle \mathbf{r}_A|\hat{R}(\xi_A)|\mathbf{r}_A\rangle+\frac{1}{2}\langle \mathbf{r}_A|\hat{G}(\xi_A)|\mathbf{r}_A\rangle$, takes on non-positive values at the points $\mathbf{r}_A$ in which $\langle \mathbf{r}_A|\hat{R}(\xi_A)|\mathbf{r}_A\rangle \leq \frac{1}{2}|\langle \mathbf{r}_A|\hat{G}(\xi_A)|\mathbf{r}_A\rangle|$ and $\langle \mathbf{r}_A|\hat{G}(\xi_A)|\mathbf{r}_A\rangle<0$ (**Figure 7**). Such points configure forbidden regions for confinement because confinement is characterized by the concentration of quantum probability configuring the observable to be measured by a square modulus detector (**Castañeda**, 2022). Nevertheless, condition $\int_M d^2\xi_A \langle \mathbf{r}_A|\hat{R}(\xi_A)|\mathbf{r}_A\rangle \geq \left|\int_M d^2\xi_A \langle \mathbf{r}_A|\hat{G}(\xi_A)|\mathbf{r}_A\rangle\right|$ for $\int_M d^2\xi_A \langle \mathbf{r}_A|\hat{G}(\xi_A)|\mathbf{r}_A\rangle<0$ must be fulfilled to ensure the achievement of Eq. (15). This means that:

(i) The set of geometric excited states of space is non-separable because the space state overlapping is required to fulfill Eq. (15).

(ii) The forbidden zones, whose modes are non-factorable quantities, are excited by the geometric potential. Indeed, the geometric potential operator in Eq. (17) takes the non-factorable form

$$\hat{G}(\xi_A)=\int_M d^2\xi_D\,|\kappa(\xi_+,\xi_-)|\left(|\Theta(\xi_+)\rangle\langle\Theta(\xi_-)|\exp(i\alpha(\xi_+,\xi_-))+|\Theta(\xi_-)\rangle\langle\Theta(\xi_+)|\exp(i\alpha(\xi_-,\xi_+))\right). \quad (18)$$

Consequently, the density operator of geometric states of space $\hat{W}(\xi_A)=\hat{R}(\xi_A)+\frac{1}{2}\hat{G}(\xi_A)$

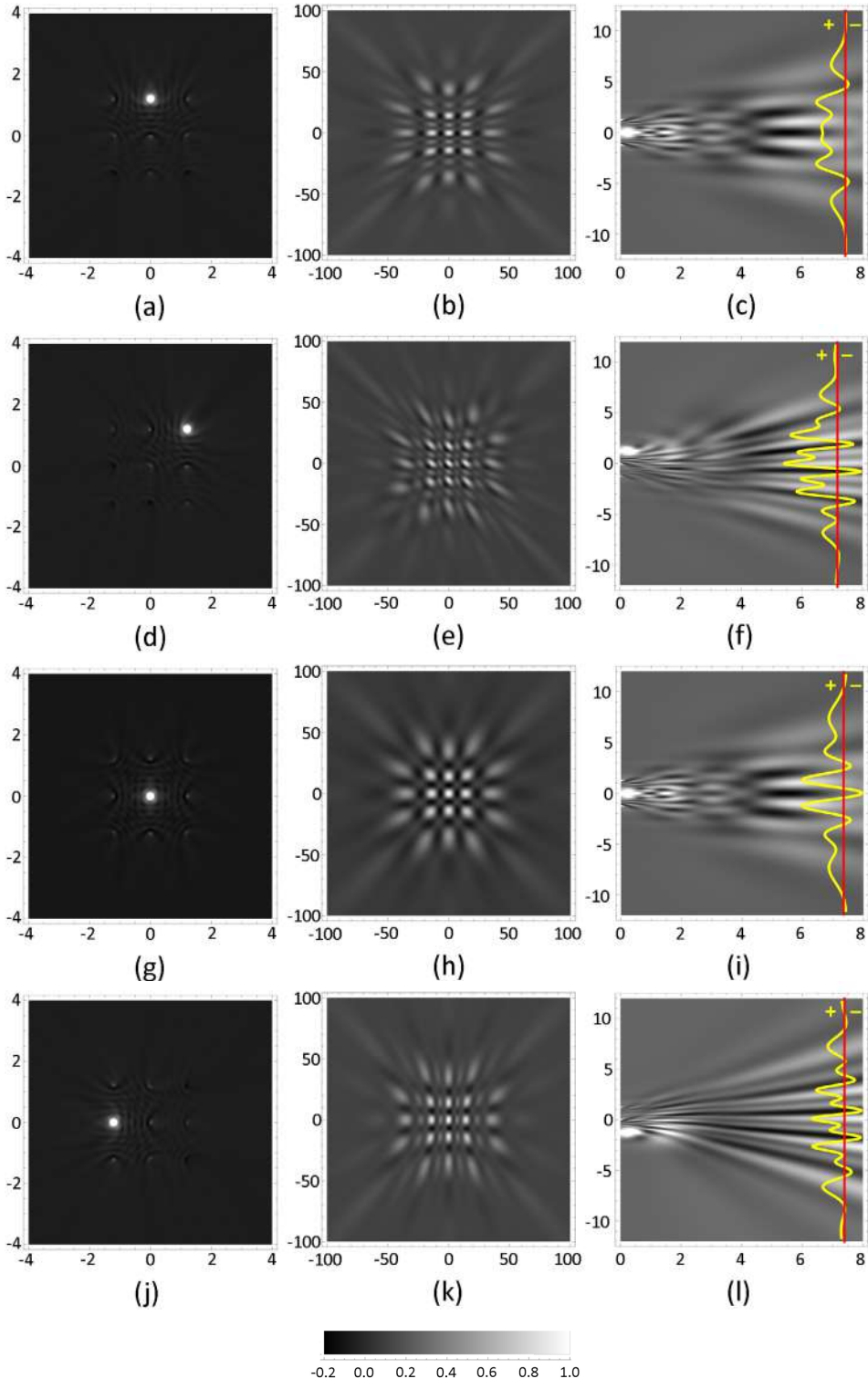

Figure 7. Cross-sections (left and central columns) and axial sections (right column) of some individual spatially structured Lorentzian wells of the example in **figure 6** (bottom row). White dots of the cross-section on the left column denote the vertex of the corresponding well.

becomes non-factorable for high non-locality values $\left|\kappa\left(\xi_{+},\xi_{-}\right)\right|$.

(iii) Forbidden zones of each geometric state of space must coincide with confinement zones of the remaining space states in such a way that the forbidden regions are removed by the addition of the space states. As a consequence, the values of the confinement zones of each geometric state of space diminish because of the negative values of the coincident forbidden zones of the remaining space states. It can be formalized without loss of generality by considering the two geometric states of space in a Young interferometer, whose vertices are placed at the mask pinholes in $\boldsymbol{\xi}_{A}=\pm\,\mathbf{a}/2$. Therefore, the inequality

$$\left\langle \mathbf{r}_{A}\left|\hat{W}\left(\mathbf{a}/2\right)\right|\mathbf{r}_{A}\right\rangle+\left\langle \mathbf{r}_{A}\left|\hat{W}\left(-\mathbf{a}/2\right)\right|\mathbf{r}_{A}\right\rangle>\left\langle \mathbf{r}_{A}\left|\hat{W}\left(\pm\mathbf{a}/2\right)\right|\mathbf{r}_{A}\right\rangle \tag{19}$$

is fulfilled except over the forbidden zones of $\left\langle \mathbf{r}_{A}\left|\hat{W}\left(\mp\mathbf{a}/2\right)\right|\mathbf{r}_{A}\right\rangle$.

These features suggest a new type of entanglement between the geometric states of space that we call spatial entanglement (**Castañeda**, 2022), (**Castañeda *et al.***, 2023). Usually, the term entanglement denotes certain interactions at a distance between photons or matter particles (**Hessmo *et al.***, 2003; **Jones & Wiseman**, 2011). In the proposed theory, this term denotes the fact that pairs of geometric states of space with vertex separation longer than the geometric uncertainty limit can modify each other's confinement zones in the absence of photons. In this sense, geometric states of space under high-valued prepared non-locality become spatially entangled at their forbidden zones.

The individual geometric states of space can be numerically modified by considering their spatial entanglement so that $\left\langle \mathbf{r}_{A}\left|\hat{W}'\left(\boldsymbol{\xi}_{A}\right)\right|\mathbf{r}_{A}\right\rangle\geq 0$ and $\left|\psi(\mathbf{r}_{A})\right|^{2}=\left\langle \mathbf{r}_{A}\left|\hat{\mathrm{H}}_{0}\right|\mathbf{r}_{A}\right\rangle=\frac{\hbar\omega}{2}\int_{M}d^{2}\xi_{A}\left\langle \mathbf{r}_{A}\left|\hat{W}'(\boldsymbol{\xi}_{A})\right|\mathbf{r}_{A}\right\rangle$. These modified space states should provide the quantum probabilities for single-photon detection in the individual experimental realizations. However, their measurement is challenging for experimentalists, mainly because of the stringent restrictions established by quantum eraser experiments (**Scully & Zubairy**, 1997), (**Rueckne & Peidle**, 2013).

Given that each geometric potential mode excites only a specific pair of space states, the modification of a set of geometric states of space should be performed by pairs. For the monomodal Young interference, the modification is performed as follows:

- $\left\langle \mathbf{r}_{A}\left|\hat{W}'\left(\pm\mathbf{a}/2\right)\right|\mathbf{r}_{A}\right\rangle=\left\langle \mathbf{r}_{A}\left|\hat{W}\left(\pm\mathbf{a}/2\right)\right|\mathbf{r}_{A}\right\rangle$ for the confinement zones, where $\left\langle \mathbf{r}_{A}\left|\hat{W}\left(\pm\mathbf{a}/2\right)\right|\mathbf{r}_{A}\right\rangle>0$.
- $\left\langle \mathbf{r}_{A}\left|\hat{W}'\left(\pm\mathbf{a}/2\right)\right|\mathbf{r}_{A}\right\rangle=0$ for the forbidden zones, where $\left\langle \mathbf{r}_{A}\left|\hat{W}\left(\pm\mathbf{a}/2\right)\right|\mathbf{r}_{A}\right\rangle\leq 0$
- $\left\langle \mathbf{r}_{A}\left|\hat{W}'\left(\pm\mathbf{a}/2\right)\right|\mathbf{r}_{A}\right\rangle=\left\langle \mathbf{r}_{A}\left|\hat{W}\left(\mathbf{a}/2\right)\right|\mathbf{r}_{A}\right\rangle+\left\langle \mathbf{r}_{A}\left|\hat{W}\left(-\mathbf{a}/2\right)\right|\mathbf{r}_{A}\right\rangle$ for the spatial entanglement zones, where $\left\langle \mathbf{r}_{A}\left|\hat{W}\left(\pm\mathbf{a}/2\right)\right|\mathbf{r}_{A}\right\rangle>0$ and $\left\langle \mathbf{r}_{A}\left|\hat{W}\left(\mp\mathbf{a}/2\right)\right|\mathbf{r}_{A}\right\rangle\leq 0$.

Figure 8 illustrates the modified geometric states of space by considering their spatial entanglement, for an array of 2x2 points at M, as well as the pattern obtained after their overlapping.

However, by suitably weakening the prepared non-locality, the forbidden regions are removed and, therefore, the spatial entanglement between the excited states of space is removed too, although the excitation provided by the geometric potential modes is yet visible, as illustrated in **figure 9.** These results show that single-photon interference without spatial entanglement is also feasible.

Theoretical description of the individual experimental realization

The theoretical term "individual experimental realization" denotes the interval for $\left\langle 1\left|\hat{n}\right|1\right\rangle=1$ of the binary sequence $\left\langle 1\left|\hat{n}\right|1\right\rangle=1$, $\left\langle 0\left|\hat{n}\right|0\right\rangle=0$ of the basic experiment segment in single-photon interference.

It is well-established that single photons can be created by local emissions resulting from atomic transitions of matter that specify its frequency ω and can be annihilated by local detection at a pixel of a square modulus detector (**Saleh & Teich**, 2019). The

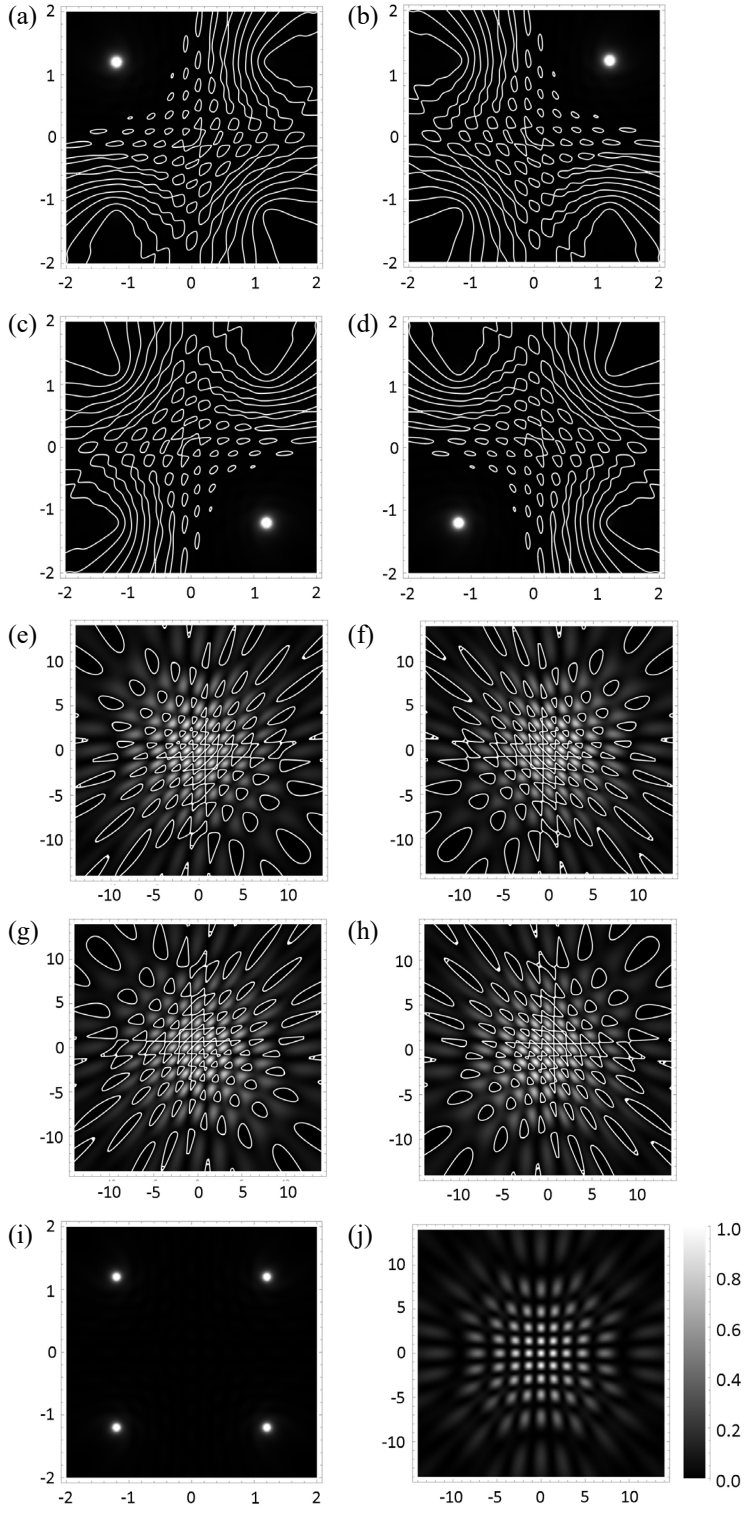

Figure 8. Cross-sections at $z = 0.1\lambda$ on the upper row and $z = 20\lambda$ on the second row ($\lambda = 0.4\mu m$) of the modified individual excited states of space by spatial entanglement in the MD stage and the complete excited state ((i), (j)) for single-photon interference with 2x2 array of points at M under high prepared non-locality. The points are placed on the vertices of a square with a side of 3λ in length. Closed contours in graphs (a)-(h) denote the forbidden zones set to null by spatial entanglement. Horizontal and vertical axes: Cartesian components of $\mathbf{r}_A$ in μm. The scale is in dimensionless arbitrary units.

Revista de la Academia Colombiana de Ciencias Exactas, Físicas y Naturales
48(189):768-783, octubre-diciembre de 2024. doi: https://doi.org/10.18257/raccefyn.2863

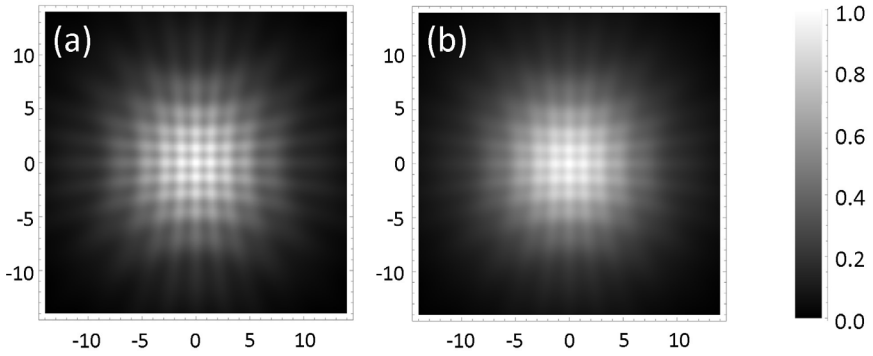

Figure 9. Cross-sections at $z = 20\lambda$ of the complete excited state for single-photon interference with the 2x2 array of points in **figure 8** under Gaussian-prepared non-locality at M with a standard deviation of **(a)** 2.7λ and **(b)** 2.4λ

photon's corpuscular nature is also well-established as a particle of quantum energy $E = \hbar\omega$ (**Mandel & Wolf**, 1995). In P&M-configured setups for single-photon interference (**Figure 1**), a photon source and a square modulus detector are placed at the S and D planes, respectively. The interference device, usually a mask, is placed at a third plane, M, between S and D. Local observables for photon emission at S and photon arrivals at M and D are determined by the quantum probabilities $\left|\psi\left(\mathbf{r}'_A\right)\right|^2 \left|t\left(\mathbf{r}'_A\right)\right|^2 \cos^2\left(\beta\left(\mathbf{r}'_A\right)\right)$ in Eq. (11), $\left|\psi\left(\xi_A\right)\right|^2$ and $\left|\psi\left(\mathbf{r}_A\right)\right|^2$ given by Eqs. (14) and Eq. (15), respectively. Therefore, the single photon of any individual experimental realization should be considered as a particle moving in the interferometer. The localizability of such a particle in the setup is restricted by both the quantum and the geometric uncertainties. However, the determination of the specific photon path is irrelevant to both the phenomenological explanation of interference and the mathematical prediction of the experimental outcomes. In contrast, the following description should be the relevant characterization of an individual experimental realization in the framework of the proposed model:

(i) The single photon locally emitted by the source with a specific quantum probability enters the ground state of space with the vertex at the emission point and moves confined in the volume of the corresponding Lorentzian well until locally arriving at any point of the interference device in the well basis.

(ii) If the arriving point is opaque, then the photon is annihilated by absorption by the device. If the arriving point is transparent, the single photon crosses the device with a specific quantum probability and enters the geometric state of space with the vertex at the crossing point.

(iii) If the prepared non-locality at M links the crossed point with other transparent points of the device, then the space state is excited by the geometric potential establishing a spatially structured Lorentzian well in the volume delimited by the interference device and the detector. The single photon moves confined in any of the confinement zones of this well until being locally measured by the detector.

This description results from a direct phenomenological interpretation of the mathematical model for which further premises or hypotheses about the corpuscular nature of the photon and its behavior in the setup have been not advanced. Therefore, the local events of source emission, mask crossing, and detector recording, and the photon confinement in the spatially structured Lorentzian well of any geometric state of space in the setup characterize the proposed theory as a corpuscular framework. By including single-matter particle interference in ordinary space −which can be explained in the same way by this theory−, the proposed corpuscular framework should motivate the community to revisit the phenomenology of the wave nature of interference.

The canonical equation for the quantum interference operator is expressed as

$$\hat{\mathrm{H}} = \hbar\omega\left(\hat{n} + \frac{1}{2}\right)\int d^2 q_A\, \hat{W}(\mathbf{q}_A), \tag{20}$$

with $\mathbf{q}_A \equiv \mathbf{r}'_A$ for the SM stage, $\mathbf{q}_A \equiv \boldsymbol{\xi}_A$ for the MD stage, and $\left[\hat{n}, \hat{W}\right] = 0$, which implies $\left[\hat{n}, \hat{R}\right] = \left[\hat{n}, \hat{G}\right] = 0$. Therefore, the canonical quantum interference operator for any individual experimental realization is

$$\left\langle 1\middle|\hat{\mathrm{H}}\middle|1\right\rangle = \hat{\mathrm{H}}_1 = \frac{3}{2}\hbar\omega\int d^2 q_A\, \hat{W}(\mathbf{q}_A). \tag{21}$$

Equation (21) points to the fact that one photon of quantum energy $E = \hbar\omega$ propagates confined in the geometrical states of space of the vacuum energy $(1/2)\hbar\omega$ established in the setup and its arrival to a plane of reduced coordinates $(\mathbf{u}_A, \mathbf{u}_D)$ is canonically described by

$$\left\langle \mathbf{u}_A\middle|\hat{\mathrm{H}}_1\middle|\mathbf{u}_A\right\rangle = \frac{3}{2}\hbar\omega\int d^2 q_A \left\langle \mathbf{u}_A\middle|\hat{W}(\mathbf{q}_A)\middle|\mathbf{u}_A\right\rangle, \tag{22}$$

with $(\mathbf{u}_A, \mathbf{u}_D) \equiv (\boldsymbol{\xi}_A, \boldsymbol{\xi}_D)$ for the SM stage and $(\mathbf{u}_A, \mathbf{u}_D) \equiv (\mathbf{r}_A, \mathbf{r}_D)$ for the MD stage. Therefore, the single photon emitted at $\mathbf{r}'_0 \equiv \mathbf{q}_0$ of S moves confined in the Lorentzian well with the vertex at this point and arrives to any point $\boldsymbol{\xi}_0 \equiv \mathbf{u}_0$ of M in accordance to $\left\langle \mathbf{u}_0\middle|\hat{\mathrm{H}}_1\middle|\mathbf{u}_0\right\rangle = \frac{3}{2}\hbar\omega\left\langle \mathbf{u}_0\middle|\hat{W}(\mathbf{q}_0)\middle|\mathbf{u}_0\right\rangle$, with $\hat{W}(\mathbf{q}_0) = \hat{R}(\mathbf{q}_0)$. The arriving point is placed within the non-locality support given by $\left\langle \mathbf{u}_0\middle|\hat{\mathrm{H}}_1\middle|\mathbf{u}_0 + \mathbf{u}_D\right\rangle = \frac{3}{2}\hbar\omega\int d^2 q_A \left\langle \mathbf{u}_0\middle|\hat{W}(\mathbf{q}_A)\middle|\mathbf{u}_0 + \mathbf{u}_D\right\rangle$ with $\hat{W}(\mathbf{q}_A) = \hat{R}(\mathbf{q}_A)$. Now, let us consider that (i) the arriving point $\mathbf{q}_0 = \boldsymbol{\xi}_0$ is transparent and (ii) there are transparent points, $\mathbf{q}_0 \pm \mathbf{q}_D$, so that the pairs $(\mathbf{q}_0, \mathbf{q}_0 \pm \mathbf{q}_D)$ belong to non-locality supports centered at $\mathbf{q}_A = \mathbf{q}_0 \pm \mathbf{q}_D/2$. Therefore, the single photon that arrives at $\boldsymbol{\xi}_0 \equiv \mathbf{q}_0$ enters the individual geometric state of space $\hat{W}(\mathbf{q}_0) = \hat{R}(\mathbf{q}_0) + (1/2)\,\hat{G}(\mathbf{q}_0)$ excited by $\hat{G}(\mathbf{q}_0) = \int d^2 q_D\, \kappa(\mathbf{q}_0, \mathbf{q}_0 + \mathbf{q}_D)\left|\Theta(\mathbf{q}_0)\right\rangle\left\langle\Theta(\mathbf{q}_0 + \mathbf{q}_D)\right|$, i.e., the geometric potential composed by the subset of modes activated by the prepared non-locality for pairs of points $(\mathbf{q}_0, \mathbf{q}_0 \pm \mathbf{q}_D)$. The single photon cannot be confined in the forbidden $\hat{W}(\mathbf{q}_0)$ zones and the probability to be confined in a spatially entangled zone given by $\hat{W}'(\mathbf{q}_0)$ is lower than the corresponding value given by $\hat{W}(\mathbf{q}_0)$. Consequently, the single photon moves in the MD stage effectively confined in the modified geometric state of space $\hat{W}'(\mathbf{q}_0)$ so that its detection by any pixel of the detector at D is described by $\left\langle \mathbf{u}_A\middle|\hat{\mathrm{H}}'_1\middle|\mathbf{u}_A\right\rangle = \frac{3}{2}\hbar\omega\left\langle \mathbf{u}_A\middle|\hat{W}'(\mathbf{q}_0)\middle|\mathbf{u}_A\right\rangle \geq 0$ where $\left\langle \mathbf{u}_A\middle|\hat{W}'(\mathbf{q}_0)\middle|\mathbf{u}_A\right\rangle$ represents the quantum probability of finding the single photon at the point $\mathbf{u}_A \equiv \mathbf{r}_A$ of D. So, the modified quantum interference operator by spatial entanglement $\hat{\mathrm{H}}'_1 = (3/2)\hbar\omega\,\hat{W}'(\mathbf{q}_0)$ describes the effective single photon confinement in the individual experimental realization represented by the modified geometric state of space $\hat{W}'(\mathbf{q}_0)$. Consequently, the canonical quantum interference operator can describe exhaustively any individual experimental realization of single-photon interference in ordinary space and points to the fact that they are not pure random events because of the deterministic Lorentzian wells in the SM stage and the spatially structured Lorentzian wells in the MD stage established by $\hat{W}'(\mathbf{q}_0)$. The statistical appearance of single-photon detections in the complete interference experiment is due to the statistics of source emissions and mask crossings, the quantum and geometric uncertainties that randomize the confinement in the established zones in each experimental realization, and the quantum sensitivity of the detector that determines its detection rate. However, this statistical appearance is compatible with the deterministic geometries of the space states established in the experimental setup.

Conclusions

The rigorously deduced quantum interference operator describes non-paraxial single-photon interference as resulting from the photon confinement in geometric states of space filtered (i.e., selected and weighted) by the setup. This exact second-order mathematical tool confers a physical meaning to geometry in interference, as relativity did for gravity. It implies an epistemological departure from the standard interference formalism based on the paraxially approximated first-order procedure of wave superposition that calls for its discussion by the community.

More precisely, in this framework, ordinary space is considered a system with geometric states provided by the vacuum, i.e., in the absence of photons and with the vacuum energy. Ground states of space can be geometrically excited (i.e., spatially modulated) by geometric potential modes. Such modes are activated by prepared non-locality functions also provided by the vacuum. This conception of ordinary space completely differs from the Newtonian passive scenario of the standard interference formalism. Indeed, the geometric states of space determine interference so that the patterns recorded as experimental outcomes are effectively space state maps performed by the single photons that move along their confinement zones.

The corpuscular framework of the proposed theory is remarkable. It also explains single matter particle non-paraxial interference, which opens the way to the community revisiting the wave nature attributed to interference. Additionally, the description does not resort to wave-particle duality and associated hypotheses to describe interference (particle delocalization, self-interference, and wave collapse, for instance). It only requires the notion of confinement as the phenomenological principle to explain interference in a generalized context (including classical light and matter particles) (**Castañeda *et al.***, 2023). Furthermore, the quantum interference operator introduces new interference features not evidenced by the standard formalism, such as geometric uncertainty and spatial entanglement.

We should emphasize that the phenomenology of the interference operator refers to ordinary space, which is the environment where interference experimentally occurs instead of exclusively calculating the probability distributions of experimental outcomes in the Hilbert space, as established in quantum mechanics. From this point of view, our model could be considered as a realistic theory, also compatible with classical light interference, by considering a significantly large number of photons emitted at a time. Given their bosonic nature, photons can occupy the geometric states of space at a time, thus filling their confinement zones. For $n>>1/2$, the interference operator gives the well-known result $n\hbar\omega$ for light irradiance (**Saleh & Teich**, 2019). Besides, the angular factors of the effective transmission $\tau_{eff}(\xi_+, \xi_-)$ lead to the fulfillment of Malus' and Fresnel-Arago's classical laws of polarization (**Born & Wolf**, 1993).

Given these attributes, the phenomenology provided by the quantum interference operator seems to be more effective than the standard formalism for explaining interference in ordinary space. From this perspective, the proposed theory opens a pertinent discussion on the foundations of interference, the review of its philosophical implications, and the performing of new experiments to examine the validity of this alternative phenomenology.

Supplementary information

See the supplementary information in https://www.raccefyn.co/index.php/raccefyn/article/view/2863/4467

Author contributions

The authors contributed equally to the discussion of the subject and the paper preparation.

Conflicts of interest

The authors declare no conflicts of interest.

Data availability

No data were generated or analyzed in the presented research.

Funding statement

This work was carried out in the framework of the *Semillero 2241 - Ciencia de la Luz* research program at Universidad Nacional de Colombia.

References

Born, M. & Wolf, E. (1993). *Principles of Optics*, 6th ed. Pergamon Press.

Bohr, N. (1935). Can quantum-mechanical description of physical reality be considered complete? *Physical Review*, *48*, 696-702.

Castañeda, R., Moreno, J., Colorado, D., Laverde, J. (2020). 3D non-paraxial kernel for two-point correlation modelling in optical and quantum interference at the micro and nanoscales. *Physica Scripta*, *95*, 065502.

Castañeda, R. (2022). Confinement and spatial entanglement: phenomenology of a new interference principle. *Revista de la Academia Colombiana de Ciencias Exactas* Físicas *y Naturales, 46* (181), 902-919.

Castañeda, R., Bedoya, P., Hurtado, C. (2023). Quantum formalism of interference as confinement in spatially structured Lorentzian wells. *Journal of Physics A: Mathematical and Theoretical, 56*, 045302.

De Martini, F., Denardo, G., Zeilinger, A. (1994). *Proceedings of the Adriatico Workshop on Quantum Interferometry*. World Scientific.

Hessmo, B., Usachev, P., Heydari, H., Bjork, G. (2003). An experimental demonstration of single photon nonlocality. *arXiv: quant-ph / 0311144v1*.

Jones, S. J. & Wiseman, H. M. (2011). Nonlocality of a single photon: paths to an EPR-steering experiment. *arXiv: 1102.5369v3* [*quant-ph*].

Mandel, L. & Wolf, E. (1995). *Optical Coherence and Quantum Optics.* Cambridge University Press.

Marshman, E. & Singh, C. (2017). Investigating and improving student understanding of quantum mechanics in the context of single photon interference. *Physical Review Physics Education Research*, *13*(1), 010117.

Mérolla, J-M., Mazurenko, Y., Goedgebuer, J-P., Rhodes, W.T. (1999). Single-Photon Interference in Sidebands of Phase-Modulated Light for Quantum Cryptography. *Physical Review Letters*, *82*, 1656.

Rueckne, W. & Titcomb, P. (1996). A lecture demonstration of single photon interference. *American Journal of Physics*, *64*(2), 184-188.

Rueckne, W. & Peidle, J. (2013). Young's double-slit experiment with single photons and quantum eraser. *American Journal of Physics*, *81*(12), 951-958.

Tang, J. & Hu, Z. B. (2022). Analysis of single-photon self-interference in Young's double-slit experiments. *Results in Optics*, *9*, 100281.

Saleh, B.E.A. & Teich, M.C. (2019). *Fundamentals of Photonics* 3rd ed. Wiley.